Enkephalin-mediated modulation of basal somatic sensitivity by regulatory T cells in mice

Nicolas Aubert [1], Madeleine Purcarea [1], Julien Novarino [1], Julien Schopp [2], Alexis Audibert [3], Wangtianrui Li [1], Marie Fornier [1], Léonie Cagnet [1], Marie Naturel [1], Armanda Casrouge [1], Marie-Caroline Dieu-Nosjean [1], Nicolas Blanchard [3], Gilles Dietrich [4], Cedric Peirs [2], Gilles Marodon [1,*]

1 Centre d'Immunologie et des Maladies Infectieuses (CIMI-PARIS), , INSERM, CNRS, Sorbonne Université, Paris, F-75013, France

2 Université Clermont Auvergne, CHU Clermont-Ferrand, INSERM, Neuro-Dol, Clermont-Ferrand F-63000, France

3 Toulouse Institute for Infectious and Inflammatory Diseases (Infinity), INSERM, CNRS, Université Toulouse III - Paul Sabatier (UPS), Toulouse, F-31000, France

4 Institut de Recherche sur la Santé Digestive (IRSD), Université de Toulouse, INSERM, INRAE, ENVT, Université Toulouse III - Paul Sabatier (UPS), Toulouse, F-31000, France

* corresponding author : gilles.marodon@inserm.fr

Abstract

$CD4^+CD25^+Foxp3^+$ regulatory T cells (Treg) have been implicated in pain modulation in various inflammatory conditions. However, whether Treg cells hamper pain at steady state and by which mechanism is still unclear. From a meta-analysis of the transcriptomes of murine Treg and conventional T cells (Tconv), we observe that the proenkephalin gene (*Penk*), encoding the precursor of analgesic opioid peptides, ranks among the top 25 genes most enriched in Treg cells. We then present various evidence suggesting that *Penk* is regulated in part by members of the TNF receptor family and the transcription factor Batf. Using mice in which the promoter activity of *Penk* can be tracked with a fluorescent reporter, we also show that *Penk* expression is mostly detected in Treg and activated Tconv in non-inflammatory conditions in the colon and skin. Functionally, Treg cells proficient or deficient for *Penk* suppress equally well the proliferation of effector T cells *in vitro* and autoimmune colitis *in vivo*. In contrast, inducible ablation of *Penk* in Treg leads to heat hyperalgesia in both male and female mice. Overall, our results indicate that Treg might play a key role at modulating basal somatic sensitivity in mice through the production of analgesic opioid peptides.

Introduction

Regulatory T-cells (Treg), characterized by the expression of the alpha chain of the interleukin-2 receptor CD25 and the transcription factor Foxp3 (Hatzioannou et al., 2021), are known to be key players in immuno-regulation in both humans and mice; too few may lead to autoimmune diseases whereas too many may prevent an efficient immune response to cancer (Kim et al., 2007; Nishikawa and Sakaguchi, 2010).

Over the last few years, several new functions of Treg beyond immunoregulation have been identified in tissue regeneration or local regulation of metabolism (Xiao et al., 2022; Meng et al., 2023; Shime et al., 2020) for instance. In addition, there is accumulating evidence of a cross-talk between Treg and the nervous system. This includes promotion of oligodendrocyte differentiation or inhibition of neuroinflammation facilitating CNS repair process after brain injuries and preventing cognitive decline (Dombrowski et al., 2017; Huang et al., 2020; Ito et al., 2019; Lemaitre et al., 2023).

Furthermore, Treg have been involved in the regulation of pain in various models of nerve injury in rats and mice, such as in autoimmune neuritis or chronic constriction of the sciatic nerve (Austin et al., 2012; Duffy et al., 2019; Kuhn et al., 2021). Depletion of Treg has been associated with enhanced pain sensitivity whereas increased Treg number or activity limit pain hypersensitivity (Lees et al., 2015). Although the current view is that Treg controls pain through their immuno-suppressive functions (Bethea and Fischer, 2021), whether Treg might regulate pain at steady state is currently unknown. Our results uncover a previously unknown function of Treg that modulates basal somatic sensitivity through the production of analgesic peptides derived from the proenkephalin *Penk* gene.

Results

A meta-signature of murine Treg

Using 11 available transcriptomes retrieved from the GEO website, we generated a Treg molecular signature at steady state in lymphoid tissues, significantly enhancing the robustness of

our analysis compared to individual studies. The 25 most differentially expressed genes are depicted in Figure 1A, with the complete list provided in Table S1. As expected from the sorting strategies used to isolate Treg (detailed in Table 1 of the Materials and Methods section), *Il2ra* and *Foxp3* emerged as the most differentially expressed genes in Treg compared to Tconv. Several well-known Treg markers such as *CTLA-4*, *Itgae* (CD103), *Ikzf2* (Helios), *Tnfrsf4* (OX40) and Tnfrsf9 (4-1BB) are also present on this list. Some genes, such as *Gpr83* and *Rgs1*, have been associated with Treg functions (Flynn et al., 2023; Lu et al., 2007) though their exact roles remain to be fully elucidated. Interestingly, the majority of genes on this list, including *Fam129a*, *Coro2a*, *Osbpl3*, and *Penk*, have unknown functions in Treg.

Penk expression in Treg of lymphoid and non-lymphoid organs and tissues

Using the Immuno-Navigator database (Vandenbon et al., 2016), which provides a batch-corrected collection of RNA quantification across numerous studies, samples and cell types, we confirm that *Penk* is highly correlated to *Foxp3* in lymphoid organs of mice (r=0.871, Figure 1B). Notably, Treg samples exhibited the highest level of both *Foxp3* and *Penk*. While it has been previously reported that Th2 and Th1 cells can express *Penk* (Boué et al., 2012), they do so to a lesser extent than Treg (Figure 1B).

Additionally, using publicly available datasets comparing Treg and Tconv, we observe that *Penk* is enriched in the thymus, where Treg are generated, and is also present in peripheral tissues such as visceral adipose fat and muscles (Figure 1C). Therefore, the enrichment of *Penk* mRNA in Treg is intrinsic to their generation and is independent of their tissue localization at steady state.

Penk mRNA expression is regulated by TNFR signaling and the BATF transcription factor

To explore possible mechanisms explaining the enrichment of *Penk* mRNA in Treg cells, we examined the Immuno-Navigator dataset to identify genes most correlated with *Penk* and with each other in Treg samples. We represent these correlations as a network where each node is a gene and each edge is a correlation above a certain threshold (Figure 2A). *Penk* expression is directly correlated to the expression of 5 genes: the TNF receptor family members, *Tnfrsf4* (OX40), *Tnfrsf9*

(4-1BB), *Tnfrsf18* (GITR), the transcription factor *Batf* and the short chain dehydrogenase/reductase family 39U member 1 *Sdr39u1*. As an illustration, we show the correlation between *Batf* and *Penk* expression in Treg samples (r=0.599, Figure 2B).

Furthermore, *Penk* is indirectly correlated with *Tnfrsf1b* (TNFR2), *Il2ra* (CD25) and *Cish*, a negative regulator of cytokine signaling. These strong correlations between several TNFR members, the transcription factor *Batf*, and *Penk* suggest a possible regulatory pathway. To explore this possibility, we reanalyzed our previously published dataset on the transcriptome of Treg stimulated with anti-CD3, anti-CD28 antibodies and TNFR agonists *in vitro* (Lubrano di Ricco et al., 2020). We observe that addition of TNFR2, OX40 or 4-1BB agonists increases *Penk* expression at 36 hours post-stimulation relative to controls (Figure 2C). Interestingly, *Batf* is also increased with TNFR agonists but at an earlier time point (18 hours). Consistent with our hypothesis, a dramatic decrease in *Penk* expression is observed in Treg lacking *Batf* (Hayatsu et al., 2017) (Figure 2D).

Furthermore, analysis of the UniBind database (Puig et al., 2021) revealed that the transcription factors Batf, Irf-4, Jun and Fosl2 (AP-1 members), RelA (NF-kB signaling), and the master Treg regulator Foxp3 have all been shown by ChIP-Seq to bind to the promoter/enhancer regions of *Penk* in various T-cell subsets (Figure S1).

Penk is predominantly expressed by Treg at steady state

Among other roles, *Batf* has been linked to tissue Treg differentiation in mice (Burton et al., 2023; Delacher et al., 2020; Hayatsu et al., 2017). Thus, we hypothesize that tissue Treg might be further enriched in *Penk* relative to lymphoid organs. To track *Penk*-expressing cells *in vivo*, we crossed a transgenic mouse model expressing Tamoxifen (TMX)-inducible Cre recombinase under the promoter of *Penk* ($Penk^{Cre\text{-}ERT2}$) with the $ROSA26^{TdTomato}$ reporter mice. In these mice, any cell that expressed *Penk* at the time of TMX administration would become permanently tagged with the tdTomato reporter a few days later.

We investigated the expression of *Penk* mRNA in various immune cell types across multiple

tissues by spectral flow cytometry, using a combination of lineage markers (Table S2) and an appropriate gating strategy (Figure S2A). To improve detection of *Penk* mRNA-expressing cells, we also used an anti-mCherry that cross-reacts with TdTomato (Figure S2B). In a UMAP representation of high-dimensional flow cytometry data, the projection of tdTomato expression (indicating *Penk* expression) aligns with the clusters of Treg and a small subset of activated $CD4^+$ T-cells in the lymph nodes (LN) (Figure 3A). Compared to LN, *Penk* expression encompasses entire clusters of Treg and activated T cells in the colon, likely due to the lower proportion of naïve T cells in this tissue (Figure 3B). Interestingly, in $CD4^+$ T-cells (Tconv and Treg), *Penk* expression is higher in the activated $CD62L^{low}$ $CD44^{high}$ fraction compared to the naive $CD62L^{high}$ $CD44^{low}$ phenotype (Figure S3). As summarized in Figure 3C, the highest frequency of *Penk*$^+$ cells is observed in Treg across all analyzed tissues, with the highest frequencies in the colon and the skin. *Penk* expression is also detected in Tconv of the colon and skin, but at lower frequencies than in Treg. All other cell types show low or undetectable *Penk* expression.

Immunosuppressive functions of Treg are unaffected by the lack of enkephalins

To test whether the lack of enkephalins in Treg impacts their suppressive function, we generated mice deficient in enkephalins in the hematopoietic compartment by grafting bone marrow from *Penk* knock-out mice in immunodeficient RAG2-KO mice. Several months after the graft, Treg were sorted from lymphoid organs and tested *in vitro* for their ability to suppress the proliferation of conventional T cells. No significant difference in the suppression of Tconv proliferation is observed between Treg proficient or deficient for *Penk* (Figure 4A). Similarly, the addition of Naloxone, an irreversible blocker of enkephalin receptors, neither abolishes nor enhances the suppressive function of normal Treg cells (Figure 4B). Additionally, both *Penk*-KO and wild-type Treg isolated from these chimeric mice equally prevented the occurrence of autoimmune colitis induced by the transfer of naive Tconv cells into RAG2-KO mice (Figure 4C).

Overall, these results indicate that enkephalins are not major players in the suppressive functions of Treg cells both *in vitro* and *in vivo*.

Heat hyperalgesia in mice deficient for Penk in Treg

To our knowledge, the analgesic function of *Penk* in Treg has never been reported. To determine if enkephalins produced by Treg affect pain at steady state, we generated mice deficient in *Penk* by crossing Tamoxifen (TMX)-inducible Cre recombinase under the control of the *Foxp3* promoter ($Foxp3^{Cre\text{-}ERT2}$) with mice transgenic for LoxP sequences flanking exon 2 of *Penk* ($Penk^{flox}$). In these mice (hereafter referred to as LOX), any cell expressing Foxp3 at the time of TMX administration would become deficient for exon 2 of *Penk* a few days later, hence lacking enkephalins.

Using flow cytometry, we observe that *Penk* mRNA expression is reduced by more than half in TMX-treated LOX mice compared to WT mice (Figure S4). Consistent with the Penk-Cre reporter mouse data, *Penk* mRNA expression is very low in non-Treg ($CD4^{+}Foxp3^{-}$ or $CD8^{+}$ cells) and does not differ significantly between LOX and WT mice. Thus, TMX treatment specifically reduces *Penk* mRNA expression in Treg cells of LOX mice.

Since exon 2 is the precursor of Met-Enkephalin, an endogenous opioid that affects thermal pain sensation (Aman et al., 2016), we evaluated the sensitivity of these mice to pain induced by heat (Figure 5). As controls, we used mice expressing the Cre recombinase and wild-type (WT) at the locus of LoxP sequences insertion. Mice were treated with TMX and evaluated for heat sensitivity at 10 different time points (four before and six after administration of TMX, 2 to 3 days apart). Under these conditions, a significant trend towards lower latency periods (indicative of heat hyperalgesia) is observed in the LOX group compared to WT mice (Figure S5A). Interestingly, the effect is not apparent until seven days after TMX administration. Before TMX administration, WT and LOX mice do not differ in their response to heat (Figure 5A). However, after TMX administration, LOX mice develop hyperalgesia compared to WT mice, with a 20 percent reduction in their median latency period from day 7 onwards ((8.1 vs. 6.6 sec.), Figure 5A). The effect of *Penk* deletion in Treg on heat hyperalgesia is sex-independent, as it is observed in both females and males (Figure S5B-C). Moreover, this thermal hyperalgesia in LOX mice is reproduced with a

different test in an independent laboratory where WT and LOX mice were sent for further behavioral tests (Figure S5D). Indeed, tests for innocuous (von Frey, cotton swab tests) and noxious (pin prick test) mechanical sensitivity, as well as light touch and proprioception (sticky tape test), fail to show any significant effect of Treg-specific *Penk* deficiency (Figure S5E-H). Importantly, TMX administration does not alter the proportions of skin Treg in LOX compared to WT mice (Figure 5B-C), indicating that hyperalgesia does not result from an altered distribution of Treg.

Given this result, we next investigated whether Treg could be localized in contact with nociceptive neurons in the skin. Interestingly, some skin Tregs marked by the GFP reporter molecule in our WT and LOX mice can be observed in close contact with free nerve endings labeled with a Calcitonin Gene-Related Peptide (CGRP)-specific mAb in the pad skin (Figure 5D). Because sensory neurons expressing CGRP are essential for noxious thermal heat, but not mechanical sensitivity (McCoy et al., 2013), this result suggests that Treg producing enkephalins could act locally on nociception.

Discussion

The proenkephalin gene *Penk* encodes the precursor of opioid peptides with analgesic properties (McLaughlin, 2013). Enriched expression of *Penk* in Treg has been previously reported in several specific contexts, including TCR-transgenic mice (Zelenika et al., 2002), UVB-exposure (Shime et al., 2020) or in the brains of mice recovering from stroke (Ito et al., 2019) but its role has never been directly addressed. We first explore the possible molecular mechanisms that may explain the preferential expression of *Penk* observed in tissue Treg. Using data mining and gene correlation analysis, we observed that TNFR and Batf might be involved in *Penk* regulation. Batf is known to regulate several genes through partnering with AP-1 and Irf-4 (Murphy et al., 2013), and we noted that several ChIP-Seq studies have reported the binding of these transcription factors in regulatory regions of *Penk*. Thus, our results support the hypothesis that TNFR signaling may regulate *Penk* expression in murine T cells through cooperation between Batf, AP-1 and/or Irf-4. Supporting this hypothesis, the AP-1 members Fos and Jun are crucial in *Penk* regulation in the

murine hippocampus (Sonnenberg et al., 1989). Additionally, analysis of Penk-Cre reporter mice led us to conclude that *Penk* mRNA is predominantly found in tissue Treg, further supporting the hypothesis that Batf might be a chief regulator of *Penk*. Although *Penk* might be preferentially expressed by activated T cells at steady state (Treg and Tconv), its distribution may be broader in an inflammatory context. Consistent with this, it has been reported that IL-4-treated macrophages are able to reduce neuropathic pain through their ability to produce opioid peptides (Celik et al., 2020; Pannell et al., 2016).

A prior study attributed a function to UVB-exposed Treg-derived *Penk* in promoting the growth of epidermal keratinocytes *in vitro* and facilitating wound-healing *in vivo* (Shime et al., 2020). Consequently, heightened heat sensitivity in the absence of Treg-derived *Penk* may result from altered keratinocyte homeostasis *in vivo*. Nevertheless, the impact of Treg-derived *Penk* on keratinocyte homeostasis *in vivo* under normal conditions has yet to be conclusively demonstrated.

Penk expression by $CD4^+$ T-cells has been linked to analgesia in murine models of visceral pain (Basso et al., 2018, 2016; Boué et al., 2014). However, the specific involvement of Treg in this process has not been investigated. Further research is required to determine the contribution of Treg-derived enkephalins in models of intestinal inflammatory pain. In neuroinflammatory settings, such as sciatic nerve constriction, the pain modulation by Treg could be contingent upon their immuno-suppressive function (Davoli-Ferreira et al., 2020; Duffy et al., 2019; Ledeboer et al., 2007; Shen et al., 2013), potentially mediated through the secretion of IL-10 or IL-35 (Davoli-Ferreira et al., 2020; Duffy et al., 2019). Contrary to this notion, our experiments rule out the possibility that hyperalgesia stemmed from a defect in the immuno-suppressive function of Treg. Instead, they strongly indicate a direct implication of enkephalins produced by Treg in nociception, revealing a novel non-immune intrinsic role of Treg in the endogenous regulation of basal somatic sensitivity.

Bibliography

Aman Y, Pitcher T, Simeoli R, Ballard C, Malcangio M. 2016. Reduced thermal sensitivity and increased opioidergic tone in the TASTPM mouse model of Alzheimer's disease. *PAIN* **157**:2285. doi:10.1097/j.pain.0000000000000644

Austin PJ, Kim CF, Perera CJ, Moalem-Taylor G. 2012. Regulatory T cells attenuate neuropathic pain following peripheral nerve injury and experimental autoimmune neuritis. *Pain* **153**:1916–1931. doi:10.1016/j.pain.2012.06.005

Baker AK, Hoffmann VLH, Meert TF. 2002. Dextromethorphan and ketamine potentiate the antinociceptive effects of mu- but not delta- or kappa-opioid agonists in a mouse model of acute pain. *Pharmacol Biochem Behav* **74**:73–86. doi:10.1016/s0091-3057(02)00961-9

Basso L, Boué J, Mahiddine K, Blanpied C, Robiou-du-Pont S, Vergnolle N, Deraison C, Dietrich G. 2016. Endogenous analgesia mediated by CD4(+) T lymphocytes is dependent on enkephalins in mice. *J Neuroinflammation* **13**:132. doi:10.1186/s12974-016-0591-x

Basso L, Garnier L, Bessac A, Boué J, Blanpied C, Cenac N, Laffont S, Dietrich G. 2018. T-lymphocyte-derived enkephalins reduce Th1/Th17 colitis and associated pain in mice. *J Gastroenterol* **53**:215–226. doi:10.1007/s00535-017-1341-2

Bethea JR, Fischer R. 2021. Role of Peripheral Immune Cells for Development and Recovery of Chronic Pain. *Front Immunol* **12**.

Boué J, Blanpied C, Djata-Cabral M, Pelletier L, Vergnolle N, Dietrich G. 2012. Immune conditions associated with CD4 + T effector-induced opioid release and analgesia. *Pain* **153**:485–493. doi:10.1016/j.pain.2011.11.013

Boué J, Basso L, Cenac N, Blanpied C, Rolli-Derkinderen M, Neunlist M, Vergnolle N, Dietrich G. 2014. Endogenous regulation of visceral pain via production of opioids by colitogenic CD4(+) T cells in mice. *Gastroenterology* **146**:166–175. doi:10.1053/j.gastro.2013.09.020

Burton O, Bricard O, Tareen S, Gergelits V, Andrews S, Roca CP, Whyte C, Junius S, Brajic A, Pasciuto E, Ali M, Lemaitre P, Schlenner SM, Ishigame H, Brown BD, Dooley J, Liston A. 2023. The tissue-resident regulatory T cell pool is shaped by transient multi-tissue migration and a conserved residency program. doi:10.1101/2023.08.14.553196

Celik M, Labuz D, Keye J, Glauben R, Machelska H. 2020. IL-4 induces M2 macrophages to produce sustained analgesia via opioids. *JCI Insight* **5**. doi:10.1172/jci.insight.133093

Davoli-Ferreira M, de Lima KA, Fonseca MM, Guimarães RM, Gomes FI, Cavallini MC, Quadros AU, Kusuda R, Cunha FQ, Alves-Filho JC, Cunha TM. 2020. Regulatory T cells counteract neuropathic pain through inhibition of the Th1 response at the site of peripheral nerve injury. *Pain* **161**:1730–1743. doi:10.1097/j.pain.0000000000001879

Delacher M, Imbusch CD, Hotz-Wagenblatt A, Mallm JP, Bauer K, Simon M, Riegel D, Rendeiro AF, Bittner S, Sanderink L, Pant A, Schmidleithner L, Braband KL, Echtenachter B, Fischer A, Giunchiglia V, Hoffmann P, Edinger M, Bock C, Rehli M, Brors B, Schmidl C, Feuerer M. 2020. Precursors for Nonlymphoid-Tissue Treg Cells Reside in Secondary Lymphoid Organs and Are Programmed by the Transcription Factor BATF. *Immunity* **52**:295-312.e11. doi:10.1016/j.immuni.2019.12.002

Dombrowski Y, O'Hagan T, Dittmer M, Penalva R, Mayoral SR, Bankhead P, Fleville S, Eleftheriadis G, Zhao C, Naughton M, Hassan R, Moffat J, Falconer J, Boyd A, Hamilton P, Allen IV, Kissenpfennig A, Moynagh PN, Evergren E, Perbal B, Williams AC, Ingram RJ, Chan JR, Franklin RJM, Fitzgerald DC. 2017. Regulatory T cells promote myelin regeneration in the central nervous system. *Nat Neurosci* **20**:674–680. doi:10.1038/nn.4528

Duffy SS, Keating BA, Perera CJ, Lees JG, Tonkin RS, Makker PGS, Carrive P, Butovsky O, Moalem-Taylor G. 2019. Regulatory T Cells and Their Derived Cytokine, Interleukin-35, Reduce Pain in Experimental Autoimmune Encephalomyelitis. *J Neurosci Off J Soc Neurosci* **39**:2326–2346. doi:10.1523/JNEUROSCI.1815-18.2019

Flynn AL, Gans J, Escobedo J, Zhu C, Florescu A-M, Shankara S, Madden SL, Kim PS, Pao LI. 2023. RGS1 Modulates Autophagic and Metabolic Programs and Is a Critical Mediator of

Human Regulatory T Cell Function. *J Immunol* **211**:1656–1668. doi:10.4049/jimmunol.2200402

Hatzioannou A, Boumpas A, Papadopoulou M, Papafragkos I, Varveri A, Alissafi T, Verginis P. 2021. Regulatory T Cells in Autoimmunity and Cancer: A Duplicitous Lifestyle. *Front Immunol* **12**.

Hayatsu N, Miyao T, Tachibana M, Murakami R, Kimura A, Kato T, Kawakami E, Endo TA, Setoguchi R, Watarai H, Nishikawa T, Yasuda T, Yoshida H, Hori S. 2017. Analyses of a Mutant Foxp3 Allele Reveal BATF as a Critical Transcription Factor in the Differentiation and Accumulation of Tissue Regulatory T Cells. *Immunity* **47**:268-283.e9. doi:10.1016/j.immuni.2017.07.008

Huang Y, Liu Z, Cao B-B, Qiu Y-H, Peng Y-P. 2020. Treg Cells Attenuate Neuroinflammation and Protect Neurons in a Mouse Model of Parkinson's Disease. *J Neuroimmune Pharmacol Off J Soc NeuroImmune Pharmacol* **15**:224–237. doi:10.1007/s11481-019-09888-5

Ito M, Komai K, Mise-Omata S, Iizuka-Koga M, Noguchi Y, Kondo T, Sakai R, Matsuo K, Nakayama T, Yoshie O, Nakatsukasa H, Chikuma S, Shichita T, Yoshimura A. 2019. Brain regulatory T cells suppress astrogliosis and potentiate neurological recovery. *Nature* **565**:246–250. doi:10.1038/s41586-018-0824-5

Kim JM, Rasmussen JP, Rudensky AY. 2007. Regulatory T cells prevent catastrophic autoimmunity throughout the lifespan of mice. *Nat Immunol* **8**:191–197. doi:10.1038/ni1428

Kuhn JA, Vainchtein ID, Braz J, Hamel K, Bernstein M, Craik V, Dahlgren MW, Ortiz-Carpena J, Molofsky AB, Molofsky AV, Basbaum AI. 2021. Regulatory T-cells inhibit microglia-induced pain hypersensitivity in female mice. *eLife* **10**:e69056. doi:10.7554/eLife.69056

Ledeboer A, Jekich BM, Sloane EM, Mahoney JH, Langer SJ, Milligan ED, Martin D, Maier SF, Johnson KW, Leinwand LA, Chavez RA, Watkins LR. 2007. Intrathecal Interleukin-10 Gene Therapy Attenuates Paclitaxel-Induced Mechanical Allodynia and Proinflammatory Cytokine Expression in Dorsal Root Ganglia in Rats. *Brain Behav Immun* **21**:686–698. doi:10.1016/j.bbi.2006.10.012

Lees JG, Duffy SS, Perera CJ, Moalem-Taylor G. 2015. Depletion of Foxp3+ regulatory T cells increases severity of mechanical allodynia and significantly alters systemic cytokine levels following peripheral nerve injury. *Cytokine* **71**:207–214. doi:10.1016/j.cyto.2014.10.028

Lemaitre P, Tareen SH, Pasciuto E, Mascali L, Martirosyan A, Callaerts-Vegh Z, Poovathingal S, Dooley J, Holt MG, Yshii L, Liston A. 2023. Molecular and cognitive signatures of ageing partially restored through synthetic delivery of IL2 to the brain. *EMBO Mol Med* **15**:e16805. doi:10.15252/emmm.202216805

Li P, Spolski R, Liao W, Wang L, Murphy TL, Murphy KM, Leonard WJ. 2012. BATF-JUN is critical for IRF4-mediated transcription in T cells. *Nature* **490**:543–546. doi:10.1038/nature11530

Lu L-F, Gavin MA, Rasmussen JP, Rudensky AY. 2007. G Protein-Coupled Receptor 83 Is Dispensable for the Development and Function of Regulatory T Cells. *Mol Cell Biol* **27**:8065–8072. doi:10.1128/MCB.01075-07

Lubrano di Ricco M, Ronin E, Collares D, Divoux J, Grégoire S, Wajant H, Gomes T, Grinberg-Bleyer Y, Baud V, Marodon G, Salomon BL. 2020. Tumor necrosis factor receptor family costimulation increases regulatory T-cell activation and function via NF-κB. *Eur J Immunol* **50**:972–985. doi:10.1002/eji.201948393

McCoy ES, Taylor-Blake B, Street SE, Pribisko AL, Zheng J, Zylka MJ. 2013. Peptidergic CGRPα Primary Sensory Neurons Encode Heat and Itch and Tonically Suppress Sensitivity to Cold. *Neuron* **78**:138–151. doi:10.1016/j.neuron.2013.01.030

McLaughlin PJ. 2013. Proenkephalin-Derived PeptidesHandbook of Biologically Active Peptides. Elsevier. pp. 1602–1609. doi:10.1016/B978-0-12-385095-9.00219-0

Meng F, Hao P, Du H. 2023. Regulatory T cells differentiation in visceral adipose tissues contributes to insulin resistance by regulating JAZF-1/PPAR-γ pathway. *J Cell Mol Med* **27**:553–562. doi:10.1111/jcmm.17680

Murphy TL, Tussiwand R, Murphy KM. 2013. Specificity through cooperation: BATF-IRF interactions control immune-regulatory networks. *Nat Rev Immunol* **13**:499–509. doi:10.1038/nri3470

Nishikawa H, Sakaguchi S. 2010. Regulatory T cells in tumor immunity. *Int J Cancer* **127**:759–767. doi:10.1002/ijc.25429

Pannell M, Labuz D, Celik M, Keye J, Batra A, Siegmund B, Machelska H. 2016. Adoptive transfer of M2 macrophages reduces neuropathic pain via opioid peptides. *J Neuroinflammation* **13**:1–17. doi:10.1186/s12974-016-0735-z

Peirs C, Williams S-PG, Zhao X, Arokiaraj CM, Ferreira DW, Noh M-C, Smith KM, Halder P, Corrigan KA, Gedeon JY, Lee SJ, Gatto G, Chi D, Ross SE, Goulding M, Seal RP. 2021. Mechanical Allodynia Circuitry in the Dorsal Horn Is Defined by the Nature of the Injury. *Neuron* **109**:73-90.e7. doi:10.1016/j.neuron.2020.10.027

Puig RR, Boddie P, Khan A, Castro-Mondragon JA, Mathelier A. 2021. UniBind: maps of high-confidence direct TF-DNA interactions across nine species. *BMC Genomics* **22**:1–17. doi:10.1186/s12864-021-07760-6

Shannon P, Markiel A, Ozier O, Baliga NS, Wang JT, Ramage D, Amin N, Schwikowski B, Ideker T. 2003. Cytoscape: A Software Environment for Integrated Models of Biomolecular Interaction Networks. *Genome Res* **13**:2498–2504. doi:10.1101/gr.1239303

Shen K-F, Zhu H-Q, Wei X-H, Wang J, Li Y-Y, Pang R-P, Liu X-G. 2013. Interleukin-10 down-regulates voltage gated sodium channels in rat dorsal root ganglion neurons. *Exp Neurol* **247**:466–475. doi:10.1016/j.expneurol.2013.01.018

Shime H, Odanaka M, Tsuiji M, Matoba T, Imai M, Yasumizu Y, Uraki R, Minohara K, Watanabe M, Bonito AJ, Fukuyama H, Ohkura N, Sakaguchi S, Morita A, Yamazaki S. 2020. Proenkephalin $^{+}$ regulatory T cells expanded by ultraviolet B exposure maintain skin homeostasis with a healing function. *Proc Natl Acad Sci* **117**:20696–20705. doi:10.1073/pnas.2000372117

Sonnenberg JL, Rauscher FJ, Morgan JI, Curran T. 1989. Regulation of proenkephalin by Fos and Jun. *Science* **246**:1622–1625. doi:10.1126/science.2512642

Vandenbon A, Dinh VH, Mikami N, Kitagawa Y, Teraguchi S, Ohkura N, Sakaguchi S. 2016. Immuno-Navigator, a batch-corrected coexpression database, reveals cell type-specific gene networks in the immune system. *Proc Natl Acad Sci* **113**:E2393–E2402. doi:10.1073/pnas.1604351113

Xiao T, Langston PK, Muñoz-Rojas AR, Jayewickreme T, Lazar MA, Benoist C, Mathis D. 2022. Tregs in visceral adipose tissue up-regulate circadian-clock expression to promote fitness and enforce a diurnal rhythm of lipolysis. *Sci Immunol* **7**:eabl7641. doi:10.1126/sciimmunol.abl7641

Zelenika D, Adams E, Humm S, Graca L, Thompson S, Cobbold SP, Waldmann H. 2002. Regulatory T Cells Overexpress a Subset of Th2 Gene Transcripts. *J Immunol* **168**:1069–1079. doi:10.4049/jimmunol.168.3.1069

Materials & Methods

Extraction of Treg meta-signatures

The datasets used were selected based on a "Treg* AND (Tconv* OR Teff*) AND Mus Musculus" search in the GEO dataset web site (https://www.ncbi.nlm.nih.gov/gds). GEO datasets were manually inspected for inclusion of studies comparing fresh Treg with fresh Tconv from lymphoid organs. Characteristics of selected datasets are summarized in Table 1. For each dataset, we generated a list of differentially expressed genes with a cutoff based on a false discovery rate (FDR) inferior to 0.05 and a log2 fold change superior to 1 with the GEO2R embedded algorithm.

Table 1: Characteristics of the datasets used for the Treg meta-signature (NA = not available; LN = Lymph Nodes)

Dataset	Genetic background	Age	Sex	Treg sorting	Tissue	Affymetrix Genome array
GSE103216	C57Bl/6	6-8 weeks	Female	Foxp3-RFP	LN	1.0
GSE136582	C57Bl/6	6-8 weeks	NA	Foxp3-GFP	Spleen	2.0
GSE14308	C57Bl/6	NA	NA	$CD25^{high}$	Spleen and LN	2.0
GSE15907	C57Bl/6	6 weeks	Male	$CD25^{high}$	Spleen	1.0
GSE17580	C57Bl/6	NA	Female	$CD25^{high}$	Mesenteric LN	2.0
GSE24210	C57Bl/6	NA	NA	$CD25^{high}$	Spleen and LN	2.0
GSE37532	C57Bl/6	25 weeks	Male	$CD25^{high}$	LN	1.0
GSE40685	C57Bl/6	NA	NA	Foxp3-GFP	Spleen and LN	2.0
GSE42021	BALB/c	NA	NA	Foxp3-GFP	Spleen and LN	2.0
GSE50096	C57Bl/6	6 weeks	NA	Foxp3-GFP	Spleen	1.0
GSE7460	C57Bl/6	32-36 weeks	NA	$CD25^{high}$	LN	2.0

Mice

All male and female mice were on a C57Bl/6J background. *Foxp3*$^{tm9(EGFP/cre/ERT2)Ayr}$/J ($Foxp3^{Cre\text{-}ERT2}$) (catalog #016961), *B6.Cg-Gt(ROSA)26Sor*$^{tm9(CAG\text{-}tdTomato)Hze}$*/J* (ROSA ^{tdTomato}) (catalog #007909), *B6.Cg-Penk*$^{tm1.1(cre/ERT2)Hze}$*/J*, ($Penk^{Cre\text{-}ERT2}$) (catalog #022862) were purchased from The Jackson Laboratory. *C57BL/6JSmoc-Penk*$^{em1(flox)Smoc}$ ($Penk^{flox}$) were purchased from Shanghai Model

Organisms (catalog NM-CKO-210032). Bone marrow from Penk-KO mice was a kind gift of Dr G Dietrich. *Penk* deficient bone marrow cells were purified from the B6.129-Penk-rs$^{tm1Pig/J}$ strain (The Jackson Laboratory, catalog #002880). For the *Penk* mapping experiments, Penk$^{Cre\text{-}ERT2}$ were bred with ROSA^{tdtomato}. All mice were confirmed to be homozygous for the inducible Cre and at least heterozygous for tdTomato by touchdown PCR (primers sequences available on request). To specifically knock-out the *Penk* gene in Tregs, Foxp3$^{Cre\text{-}ERT2}$ were crossed with Penk^{flox} leading to double heterozygous mice (F1) that were crossed together resulting in double homozygous F2 littermates. All mice used in this study were of F3 generation. Mice were genotyped by touchdown PCR (primers sequences available on request). Tamoxifen (ThermoFisher, Les Ulis, France) was dissolved in peanut oil at the concentration of 40 mg/ml under 37°C agitation and delivered by 200µL oral gavage. All mice were administered tamoxifen only once. Mice were housed under specific pathogen-free conditions and were used for experiments at 8 weeks or older. Mice were exposed to a 12-hour light and 12-hour dark cycle. Protocols are approved by the Ethics Committee for Animal Experimentation Charles Darwin (APAFIS #32284-2021070513305185 v5 and #11837-2017101816028463 v5).

Preparation of cell suspensions

Organs were harvested on ice in PBS 3% fetal calf serum (FCS). Inguinal, brachial and mesenteric LNs and spleens were directly mashed through a 70µm filter and suspended in PBS 3% FCS. Lungs, colons, livers, VAT and skin were dissected, minced then incubated in appropriate digestion buffers (Miltenyi Biotec, Paris, France) at 37°C for various duration according to manufacturer protocols. Cell suspensions were then passed through a 70µm cell strainer and suspended in PBS 3% FCS. To eliminate dead cells and debris, liver cell suspensions were isolated on a 70:30 Percoll gradient. Rings were collected, washed, and cell pellets were suspended in PBS 3% FCS. ACK Lysing Buffer was used to eliminate red blood cells in the lungs, livers and spleens (lysis performed for 1 min at RT, followed by two washes with PBS), prior to staining for flow cytometry.

Antibodies and flow cytometry analysis

The monoclonal antibodies (mAb) and fluorescent reagents used in this study are listed below in the Table. Up to 4.10^6 cells were incubated for 30 min at 4°C with fixable live/dead dye and with the anti-CD16/CD32 (clone 2.4G2) to block FcgRII and FcgRIII receptors. Cells were then stained with a combination of antibodies. Cell-surface staining was performed in PBS 3% FCS for 20 min at 4°C. Permeabilization and intracellular staining was performed using the Foxp3/Transcription Factor Staining Buffer Set kit and protocol (ThermoFisher). Stained cells were washed with PBS 1X before acquisition on a Cytek Aurora flow cytometer (Cytek Bioscience, Fremont, CA, USA). UMAPs were generated using FlowJo software, version 10.8.1 (TreeStar, Ashland, OR, USA).

Flow-FISH staining

Frozen splenocytes were thawed and washed once in complete RPMI (GIBCO) supplemented with 10% vol/vol FCS (GIBCO). Flow-FISH staining was performed using the PrimeFlow RNA Assay Kit (Invitrogen) and the subsequent anti-mouse Penk probes set (Invitrogen #PF-204) according to manufacturer's protocol. For flow cytometry staining, after Fc receptor saturation (anti-mouse CD16/32, clone 93, 1:50, Biolegend) and dead cells detection (Fixable Viability Dye, 1:1000, Invitrogen), cells were surface labelled for 30min on ice with the following antibodies : CD8a-BV421 (Clone 53-6.7, 1:200, BD Biosciences), CD44-BV605 (Clone IM7, 1:200, BD Biosciences), CD3e-BV711 (Clone 145-2C11, 1:50, Biolegend), CD4-PE-CF594 (Clone RM4-5, 1:800, BD Biosciences), CD62L-PE-Cy7 (Clone MEL-14, 1:300, BD Biosciences). Intracellular staining with Foxp3-PE antibody (Clone NRRF-30, 1:100, eBioscience) was performed after fixation and permeabilization with the reagents provided in the kit. A second fixation was performed with the reagents provided in the kit before proceeding to the FISH staining. For FISH staining, cells were incubated with the anti-mouse Penk probes set (1:20) for 2h at 40°C. After washes, cells were kept overnight at 4°C in wash buffer containing RNase inhibitors. The day after, amplification steps were performed to increase the signal : cells were first incubated with pre-amplification mix during 1.5h at 40°C, washed and then incubated with amplification mix for an additional 1.5h at 40°C. Cells were then incubated with the label probes (Alexa Fluor 647, 1:100) for 1h at 40°C. Data were

acquired on a 4-lasers LSR-Fortessa (BD Biosciences) and fcs files were analyzed with FlowJo as above.

***In vitro* and *in vivo* suppression assay**

Cells from the spleen and the lymph nodes of Foxp3-GFP mice were isolated and enriched for T-cells with LS column (Miltenyi) using anti-CD19-biotin, aCD11b-biotin and anti-Ter119-biotin. Afterward, enriched T-cells were stained with anti-CD4 PE and anti-CD62L (AF700) and sorted as $CD62L^{+}CD4^{+}$ GFP+ (Treg) or GFP- (Tconv) fractions on a FACS Aria III (BD, France). Then, Tconv and Treg were labeled with CellTrace Violet and CFSE (Thermofisher) respectively before the culture. For T-cell activation, either CD3/CD28 DynaBeads (Thermofisher) or soluble anti-CD3 (1µg/mL) + splenocytes from $Rag2^{-/-}$ mice were used. When specified, Naloxone hydrochloride (Tocris) was added to the media at the indicated concentration at the beginning of the culture. At the end of the culture, cells were stained with eF780 Fixable Viability Dye before acquisition on LSR Fortessa (BD Biosciences). To induce colitis, C57Bl/6 $Rag2^{-/-}$ mice were intraperitoneally injected with $CD4^{+}CD62L^{hi}GFP^{-}$ naive T cells (4×10^{5} cells per mouse) isolated from spleens and lymph nodes of wild-type C57Bl/6 Foxp3-GFP mice (kind gift of Dr B . Salomon), together with or without $CD4^{+}CD25^{hi}CD62L^{hi}$ Treg cells (2×10^{5} cells per mouse) isolated from spleens of $Rag2^{-/-}$ mice reconstituted with bone marrow cells of Penk-WT or Penk-KO mice.

Immunofluorescence

Mice were anesthetized with a mix of 100 mg/kg ketamine and 20 mg/kg xylazine, decapitated with scissors and the glabrous skin of the hindpaw harvested. The skin was then fixed with paraformaldehyde 4% for 2h at room temperature (RT). Fixed tissue was cryoprotected in 30% sucrose containing 0.05% sodium azide diluted in phosphate-buffered saline (PBS) at 4°C for 48h, and cut with a cryostat (Microm HM550) into 25 µm sections placed directly onto gelatine coated slides. For fluorescent immunostaining, slides were washed with PBS and blocked with 1% Bovine Serum Albumin (BSA) in PBS + 0.2% triton-X (PBS-T) for 1 hour at room temperature (RT), then incubated with primary antibodies diluted in PBS-T overnight at 4°C. Sections were then washed in

PBS and incubated with secondary antibodies diluted 1:1000 in PBS-T, for 2 hours at RT. Slices were finally washed in PBS and cover-slipped with Fluoromount-G containing DAPI (Invitrogen 00-4959-52). The following primary antibodies were used for immunofluorescence staining at the following dilutions: anti-GFP raised in rabbit (1:1000; Chromotek PABG-1), anti-CGRP raised in goat (1:500; Bio-Rad 1720-9007). We also used the following secondary antibodies: anti-rabbit conjugated with Cy3 raised in donkey (Jackson, 711-165-152), anti-rabbit conjugated with Alexa-488 raised in donkey (Jackson, 711-545-152), anti-goat conjugated with Cy5 raised in donkey (Jackson, 705-175-147). Images were obtained by epifluorescent microscopy with a motorized fluorescence microscope Axio Imager M2 equipped with a camera Axiocam 705 (Zeiss). Skin slices were imaged using a Colibri 7 light source, 10x/0.30 and 63x/1.25 objectives and the following filters from Zeiss: 02 DAPI, 38 HE eGFP, 43 HE DsRed and 50 Cy5 BP640/30. Images were generated with Zen blue 3.4 (Zeiss) and brightness and contrast adjusted using ImageJ/Fiji.

Behavioral tests

The methods used were described by Baker and collaborators (Baker et al., 2002) and by Peirs and collaborators (Peirs et al., 2021).

Heat sensitivity

For the hot plate test, the BIO-CHP apparatus was used (BIOSEB, France). Mice were placed on a metal plate maintained at 55°C. The response latency, which is the time taken to observe a nocifensive behavior such as jumping, licking or flicking of the hind paws, was recorded. The mice were then immediately removed from the plate upon the recording of a reaction, or within 25s if no response was observed to prevent tissue damage. The test was repeated every two days for a total of four measures before the administration of tamoxifen and four measures starting from D3 post-tamoxifen. Mice remained in their home cage except when being tested on the hot plate. The experimenter was blind to the genotype of the mice until the end of the experiment. Noxious heat sensitivity was independently assessed in the Neurodol laboratory with an Hargreaves test. Animals were placed in an acrylic chamber on a heated (30°C) glass plate and acclimated to the test chamber

for 30 min during 2 days and then for 30 minutes on the 3rd day prior to testing. Using a plantar analgesia meter (IITC, 40% intensity), a radiant heat source of constant intensity was focused on the plantar surface of the hind paw and the latency of paw withdrawal measured. The heat source was stopped upon paw withdrawal with a cutoff of 20 s to avoid injury. Heat sensitivity test was repeated 3 times on each hind paw with a 5-min interval between tests and the results for each paw were averaged together.

Static mechanical sensitivity

Static mechanical sensitivity was assessed with a von Frey test. Briefly, mice were habituated to transparent Plexiglas chambers on an elevated wire mesh table for at least 30 minutes for two days, and prior to testing. Assessments were performed using a set of calibrated von Frey monofilaments using the Up-Down method, starting with the 0.4 g filament. Each filament was gently applied to the plantar surface of the hind paw for 3 s or until a response such as a sharp withdrawal, shaking or licking of the limb was observed. Rearing or normal ambulation during filament application were not counted. Filaments were applied at five-minute intervals until the threshold was determined. The 50% paw withdrawal threshold (PWT) was determined for each mouse on both hind paws.

Dynamic mechanical sensitivity

Dynamic mechanical sensitivity was assessed with the Cotton swab test. Briefly, animals were habituated to transparent Plexiglas chambers on an elevated wire mesh table as described above. The head of a cotton swab was teased and puffed out with forceps until it reached approximately three times its original size. Tests were performed by lightly moving the cotton swab across the surface of the hind paw from heel to toe. If the animal reacted (lifting, shaking, licking of the paw) a positive response was recorded. A negative response was recorded if the animal showed no such behavior. The application was repeated 6 times with a 5-minute interval between applications, and a percentage of positive responses was determined. Paw withdrawal frequency (PWF) was determined for both hind paws of each mouse.

Noxious mechanical sensitivity

Noxious mechanical sensitivity was assessed with the pinprick test. Animals were acclimated to transparent Plexiglas chambers placed on a wire mesh table as described above. A small insect pin (tip diameter = 0.03 mm) was applied 10 times with a 5-minute interval between applications on the plantar side of each hind paw. Care was taken to apply a minimal pressure without penetrating the skin. If the animal showed aversive behavior (lifting, shaking, licking of the paw) a positive response was recorded. A negative response was recorded if the animal showed none of these reactions within 1 seconds of application and a percentage of positive responses were determined. Paw withdrawal frequency (PWF) was calculated by averaging the positive responses for each mouse for each hind paws.

Proprioception test

Animals were placed in an empty plastic cage and allowed to acclimate for 15-20 minutes. A 8mm diameter adhesive paper circle was then applied to the plantar surface of the hind paw covering the footpads, and the animals were immediately placed back in the chamber. The animals were observed until they demonstrated a behavioral response to the adhesive tape, and the latency in seconds to respond was recorded. Inspection of the paw, shaking of the paw or attempting to remove the tape were all considered valid responses. Each animal was habituated 1 time the day prior testing, and then tested 3 times with a 5-minute interval between tests, and the three values averaged for each animal for each hind paws.

Statistical analysis

All statistical tests are reported in the figure legends and were performed with Prism v9.4.1 (Graph Pad Inc, La Jolla, CA, USA). The statistical power of the analyses (alpha) was set at 0.05. No a priori sample size estimation based on beta power (1-alpha) was performed.

Fundings

This study was funded by research grants from Sorbonne University (SU) (Emergence 2021), la Ligue Nationale contre le Cancer (LNC) to GM, and by the National Institute for Health and Medical Research (INSERM). NA was supported by a doctoral fellowship from Fondation ARC and by a postdoctoral fellowship from EGLE TX, MF by a doctoral fellowship from the French Ministère de l'Enseignement Supérieur et de la Recherche, AA by a doctoral fellowship from the French Ministère de l'Enseignement Supérieur et de la Recherche and a 4th year extension from Fondation pour la Recherche Médicale (FRM), MP and MN by pre graduates fellowships from SU and EGLE TX respectively. MN is supported by a doctoral fellowship from the IUC of SU. JN is supported by a postdoctoral salary from the LNC. The funders had no role in the supervision of the research, in the analysis or interpretation of the results.

Acknowledgments

The authors would like to express their deepest gratitude to Dr Stéphane Melik-Parsadaniantz for the kind gift of essential tools used in this study and to Pr Radhouane Dallel (NeuroDol, UCA) for his help in setting up the collaboration. We would like to thank Olivier Brégerie, Flora Issert, Doriane Foret, Claire Lacoste (UMS 28, Paris) and Sylviane Rousselin (Neurodol, Clermont- Fd) for taking care of our mice and for their support filling ethical applications; Dr Morgane Hilaire (CIMI-PARIS) and Amélie Descheemaeker (NeuroDol) for technical help, Anne-Marie Gaydier for secretarial assistance, Francois-Xavier Lejeune (ICM, Paris) for help with biostatistics analysis, Dr Jean-Luc Teillaud for critical review of the manuscript and Dr Benoit Salomon for providing $Foxp3^{Cre\text{-}ERT2}$, $ROSA^{tdTomato}$, and $Foxp3^{GFP}$ mice and for many years of enjoyable collaborations and discussions.

Figure legends

Figure 1: A meta signature of murine Treg and *Penk* mRNA expression in lymphoid and non-lymphoid organs. A) Top 25 genes enriched in Treg compared to Tconv from lymphoid tissue from at least 10 of the 11 datasets analyzed ranked by fold change (LogFC) of mean expression relative to Tconv. The *Penk* gene is highlighted in red. **B)** Correlation of *Penk* and *Foxp3* expression in all the cell types listed in the legend according to the Immuno-navigator dataset. The Pearson correlation coefficient is indicated. Each dot is a sample, color coded as a subset according to the legend. **C)** Expression of *Penk* in Treg (blue) and Tconv (red) isolated from thymus, visceral adipose tissue (VAT) and muscle. The source of the data is indicated below each graph.

Figure 2: *Penk* expression is regulated by TNFR signaling and the BATF transcription factor. A) A network of the genes most correlated to *Penk* in Treg is shown. The Pearson correlation values were extracted from the Immuno-Navigator database (selecting only Treg in the analysis) and integrated into Cytoscape v3.7 (Shannon et al., 2003). Each node is a gene linked by edges with width proportional to the Pearson correlation. (edge range: 0.538-0.758). **B)** Illustration of the correlation between expression of *Penk* and *Batf* in Treg. Each dot is a sample from the Immuno-Navigator database. The Pearson correlation coefficient is indicated on the figure. **C)** *Penk* and *Batf* mRNA expression after *in vitro* stimulation of purified Treg with the indicated TNFR agonists prior (0), and at 18 and 36 hrs after stimulation. Each dot is a biological replicate from a single experiment. **D)** GEO2R analysis of the GSE89656 dataset between wild type control Treg (WT) and BATF-KO Treg.

Figure 3: *Penk* is predominantly expressed by Treg at steady state. A-B) (Left) UMAP representing all major cell types indicated in the figures determined by flow cytometry from lymph nodes (A) and colon (B). **(Right)** Projection of tdTomato expression on the UMAP of lymph nodes and colon. Subsets were manually gated as depicted in Figure S1A. **C)** Bubble plot displaying the average population size and frequencies of Penk^{+} cells for the listed cell populations and organs. Population size was calculated as the percentage out of total CD45^{+} single cells and represented on

a log10 scale. (n = 3 mice for the VAT, spleen and bone marrow, n = 6 mice for the other groups; results cumulative of two independent experiments).

Figure 4: Immunosuppressive functions of Treg are unaffected by the lack of enkephalins. A) In vitro suppression of WT Tconv proliferation by WT or Penk KO Tregs. **B)** In vitro suppression of WT Tconv proliferation by Penk WT Tregs in presence of Naloxone. **C)** Body weight and **D)** survival of Rag2$^{-/-}$ mice transferred with Tconv and Treg from Penk-WT or Penk-KO chimeric mice (2:1 ratio), as described in the methods. All data are cumulative of 2 independent experiments.

Figure 5: Heat hyperalgesia in mice deficient for *Penk* in Treg. A) Withdrawal latency of WT and LOX mice before (baseline) and after administration of Tamoxifen (TMX). Each dot corresponds to the mean latency response (in seconds) of 4 measurements taken before TMX administration (baseline) and 4 measurements taken from day 7 onwards (TMX). Statistical modeling was performed using a non-parametric unpaired Mann-Whitney t-test with multiple corrections. The results shown in this figure are cumulative from two independent experiments with a total of 44 mice (26 WT and 18 LOX). Each dot is a mouse. **B)** Representative flow cytometry contour plot of CD25 and Foxp3 staining on pad skin CD45^{+}CD3+CD4+ cells from WT or LOX mice 17 days after TMX gavage. **C)** Quantification of the frequency of Treg (Foxp3^{+}CD25^{+}) among CD4^{+} T cells in WT and LOX mice pad as shown in (B). The indicated p value was determined by a Mann-Whitney test. Each dot is a mouse from a single experiment. **D)** Immunofluorescence staining of CGRP neurons (red), Foxp3-GFP cells (green), and DAPI (blue) of footpad skin section of a female LOX mouse (scale bar represents 50µm). The right panel is the magnification of the area indicated on the left panel.

Supplementary figures and tables

Figure S1: Analysis of Regulatory Regions of the *Penk* gene. (Ref Seq) The location and transcription orientation of the *Penk* gene on chromosome 4 is indicated. (ENCODE cCREs) The locations of ENCODE candidate cis-regulatory regions (cCREs) are shown. Colors indicate promoter-like signature (red) and proximal enhancer-like signature (orange). (Remap density) Density representation of transcription factor binding sites at the indicated locations with filtering on T cell subsets only (source: UniBind 2021). Specific tracks depicted on the left were added to the reference genome assembly mm10 as bed files extracted from the TFBS tool in UniBind, focusing the analysis on the region flanking the cCREs depicted above. The figure was generated with the Ensembl web browser.

Figure S2. Mapping *Penk* expression in multiple tissues and cell types. A) Representative flow cytometry profiles in the spleen at day 7 post TMX administration into Penk$^{Cre\text{-}ERT2}$x ROSA^{tdtomato} mice. **B)** Representative staining of TdTomato and mCherry in the spleen at day 7 post TMX administration.

Figure S3. *Penk* expression in Tconv and Treg according to activation status in lymph nodes. Representative staining of TdTomato and mCherry in naive (CD62L^{high} CD44^{low}), central memory (CD62L^{high} CD44^{high}) and effector memory (CD62L^{low} CD44^{high}) Tconv (top) and Treg (bottom) in the lymph nodes one week post-TMX administration.

Figure S4: Specific deletion of *Penk* in Treg of LOX mice after TMX administration. A) Representative flow cytometry profiles of splenocytes in FoxP3$^{Cre\text{-}ERT2}$ x Penk$^{+/+}$ (WT) and FoxP3$^{Cre\text{-}ERT2}$ x Penk$^{fl/fl}$ mice (LOX). **B)** Frequencies of Penk^{+} cells in different CD4+ T cell populations: Treg (FoxP3^{+}), Tconv (FoxP3^{-}) and CD8^{+} T cells. Cumulative data from mice analyzed at day 3, 7, and 30 post-TMX are shown. Each dot is a mouse. Statistical modeling was performed using two-way ANOVA with multiple tests correction. ns=not significant ($p>0.05$)

Figure S5. Heat hyperalgesia in WT and LOX mice . **A)** Each dot represents the mean (± SEM) latency to heat stimulation for all mice of either WT (blue) or LOX (red) genotype. Results are

plotted as a function of days relative to TMX gavage (D0). Statistical modeling of the results was performed using linear regression curve fitting with intercept and slope comparisons. The low p-value allows the hypothesis that one curve fits all data sets to be rejected. **B-C)** Each dot is the mean value of the latency period in response to 55°C exposition for female and male mice of either WT (blue) or LOX (red) genotype for 4 baselines **(B)** and 4 post-TMX time points after D7 **(C)**. Each dot is a mouse. **D)** Withdrawal latency of WT and LOX mice before (baseline) and after TMX administration (TMX) in response to the Hargreave test. Each dot is a mouse. **E)** Each dot is the 50% paw withdrawal threshold (PWT) for all mice on both hind paws of the WT (blue) or LOX (red) genotype in response to the von Frey test at baseline or post-TMX time points. **F)** Paw withdrawal frequency (PWF) for all mice on both hind paws of the WT (blue) or LOX (red) genotype in response to the cotton swab test. Baseline and post-TMX time points are shown for each mouse. **G)** Paw withdrawal frequency (PWF) for all mice on both hind paws of the WT (blue) or LOX (red) genotype in response to the pinprick test before and after TMX gavage. **H)** Latency period in response to sticky tape test stimulation for all mice of the WT (blue) or LOX (red) genotype. Baseline and post-TMX time points are shown for each mouse hind paw. Statistical modeling was performed using Mann-Whitney tests with multiple tests correction with n = 44 (26 WT and 18 LOX) for A-C and n = 12 (6 WT and 6 LOX) for D-H. The q values indicated on the graphs are the results of the two-stage step-up FDR multiple test correction.

Table S1: List of the differentially expressed genes between Tconv and Treg. Only genes upregulated in 10 out of 11 datasets are presented with the associated log2 fold change as determined by GEO2R. (NA = not available)

Table S2: Panel of monoclonal antibodies used for flow cytometry. Indicated are the specificity, the fluorescent dye, the manufacturer, the clone and the dilution of the mAb used to generate results of figure 3.

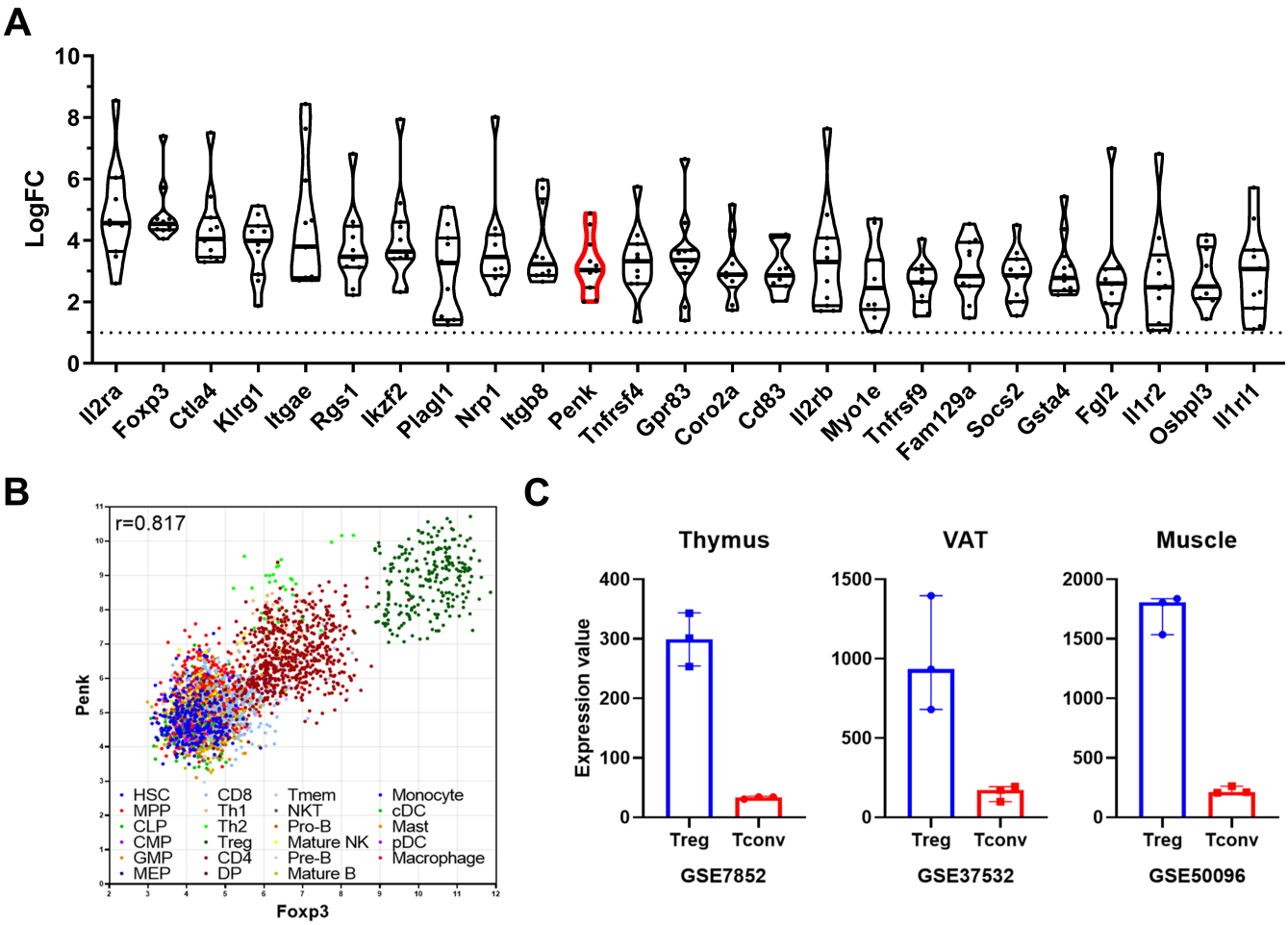
A
LogFC
10
8
6
4
2
0
Il2ra
Foxp3
Ctla4
Klrg1
Itgae
Rgs1
Ikzf2
Plagl1
Nrp1
Itgb8
Penk
Tnfrsf4
Gpr83
Coro2a
Cd83
Il2rb
Myo1e
Tnfrsf9
Fam129a
Socs2
Gsta4
Fgl2
Il1r2
Osbpl3
Il1rl1
B
r=0.817
Penk
Foxp3
HSC
MPP
CLP
CMP
GMP
MEP
CD8
Th1
Th2
Treg
CD4
DP
Tmem
NKT
Pro-B
Mature NK
Pre-B
Mature B
Monocyte
cDC
Mast
pDC
Macrophage
C
Thymus
VAT
Muscle
Expression value
400
300
200
100
0
1500
1000
500
0
2000
1500
1000
500
0
Treg
Tconv
GSE7852
GSE37532
GSE50096

Figure 1

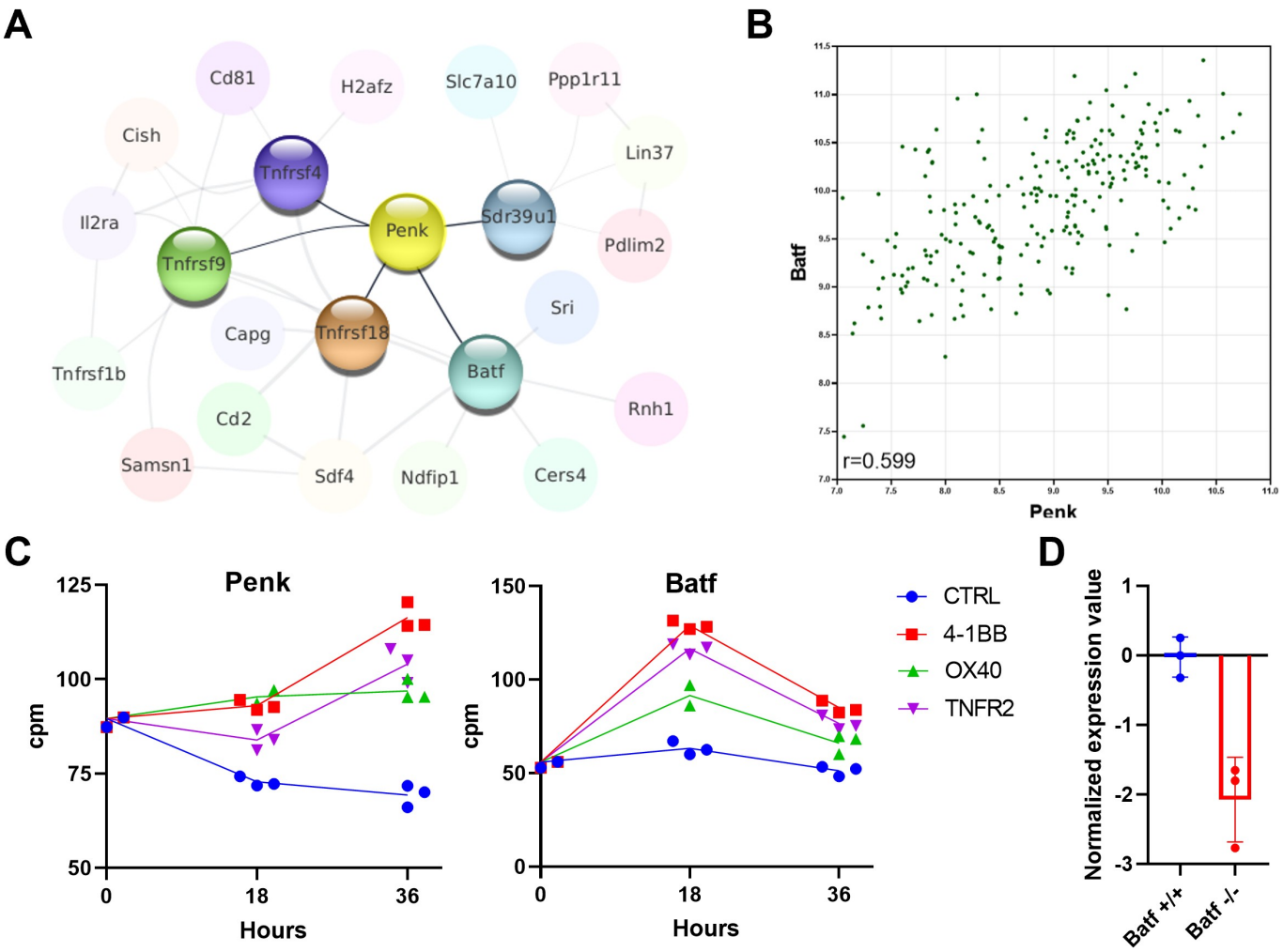
A
Cd81
H2afz
Slc7a10
Ppp1r11
Cish
Lin37
Tnfrsf4
Il2ra
Penk
Sdr39u1
Pdlim2
Tnfrsf9
Sri
Capg
Tnfrsf18
Tnfrsf1b
Batf
Rnh1
Cd2
Samsn1
Sdf4
Ndfip1
Cers4
B
Batf
Penk
r=0.599
C
Penk
Batf
cpm
Hours
CTRL
4-1BB
OX40
TNFR2
D
Normalized expression value
Batf +/+
Batf -/-

Figure 2

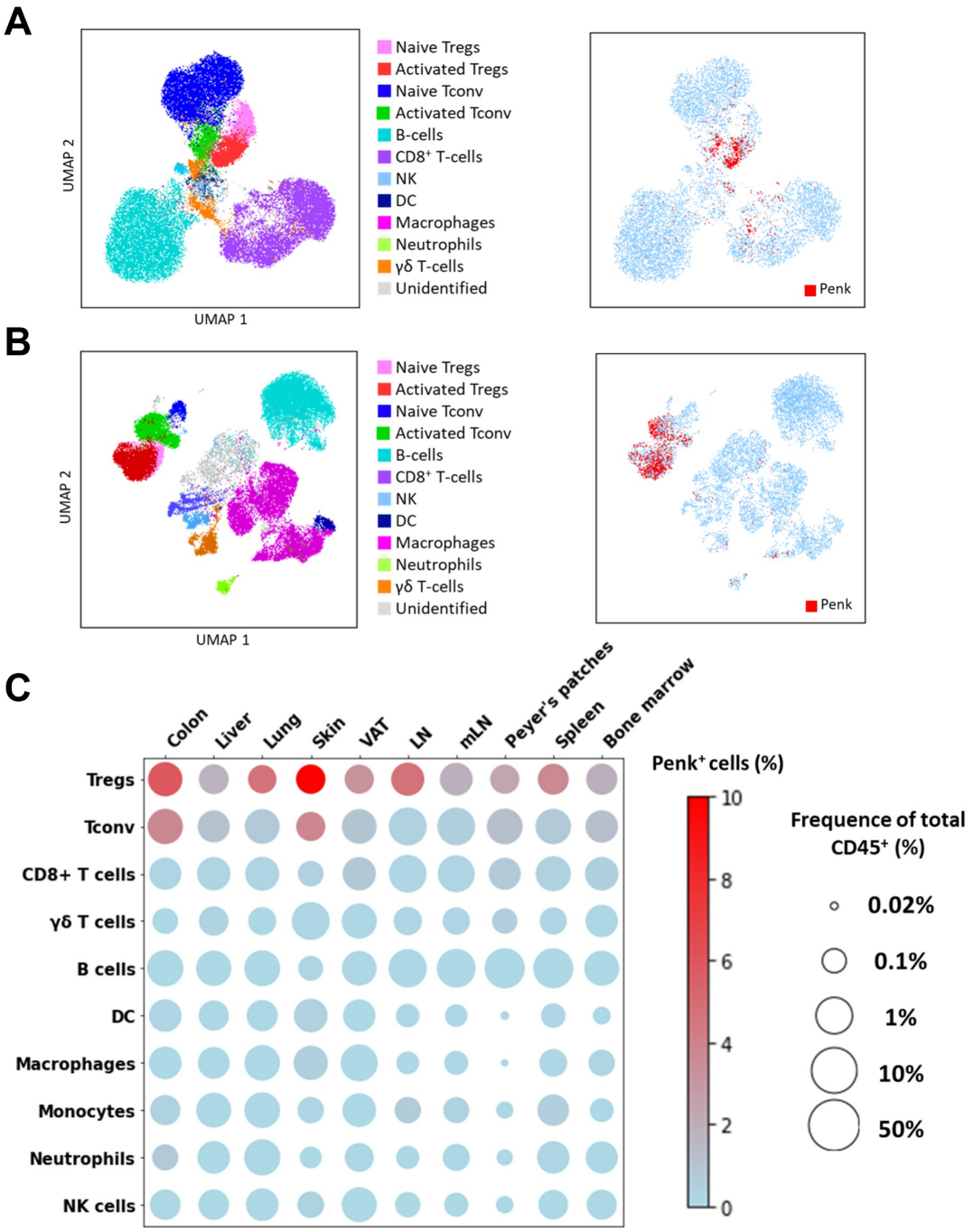
A
UMAP 2
UMAP 1
Naive Tregs
Activated Tregs
Naive Tconv
Activated Tconv
B-cells
CD8⁺ T-cells
NK
DC
Macrophages
Neutrophils
γδ T-cells
Unidentified
Penk
B
UMAP 2
UMAP 1
Naive Tregs
Activated Tregs
Naive Tconv
Activated Tconv
B-cells
CD8⁺ T-cells
NK
DC
Macrophages
Neutrophils
γδ T-cells
Unidentified
Penk
C
Colon
Liver
Lung
Skin
VAT
LN
mLN
Peyer's patches
Spleen
Bone marrow
Tregs
Tconv
CD8+ T cells
γδ T cells
B cells
DC
Macrophages
Monocytes
Neutrophils
NK cells
Penk⁺ cells (%)
10
8
6
4
2
0
Frequence of total CD45⁺ (%)
0.02%
0.1%
1%
10%
50%

Figure 3

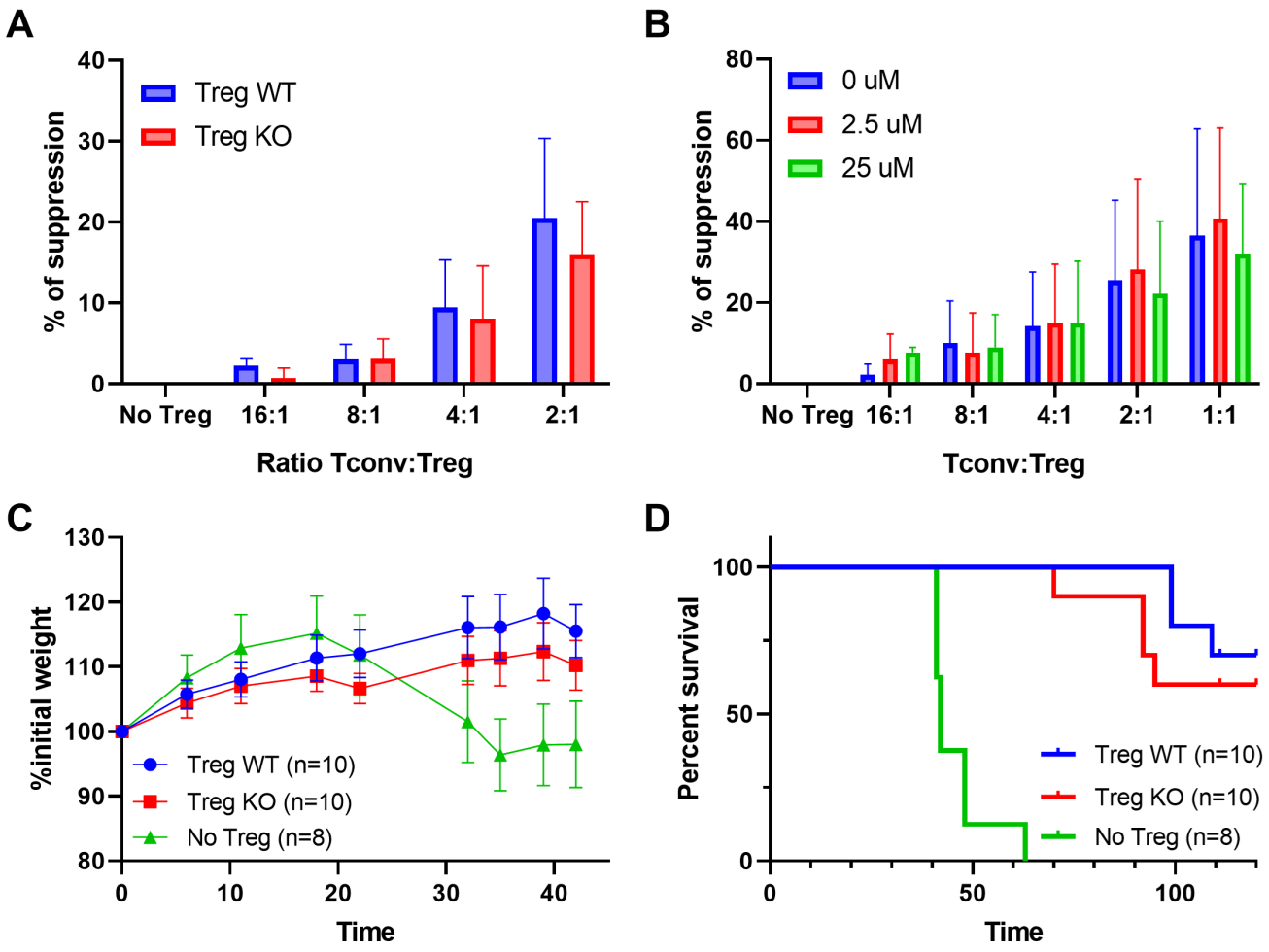
A
% of suppression
Treg WT
Treg KO
No Treg
16:1
8:1
4:1
2:1
Ratio Tconv:Treg
B
% of suppression
0 uM
2.5 uM
25 uM
No Treg
16:1
8:1
4:1
2:1
1:1
Tconv:Treg
C
%initial weight
Treg WT (n=10)
Treg KO (n=10)
No Treg (n=8)
Time
D
Percent survival
Treg WT (n=10)
Treg KO (n=10)
No Treg (n=8)
Time

Figure 4

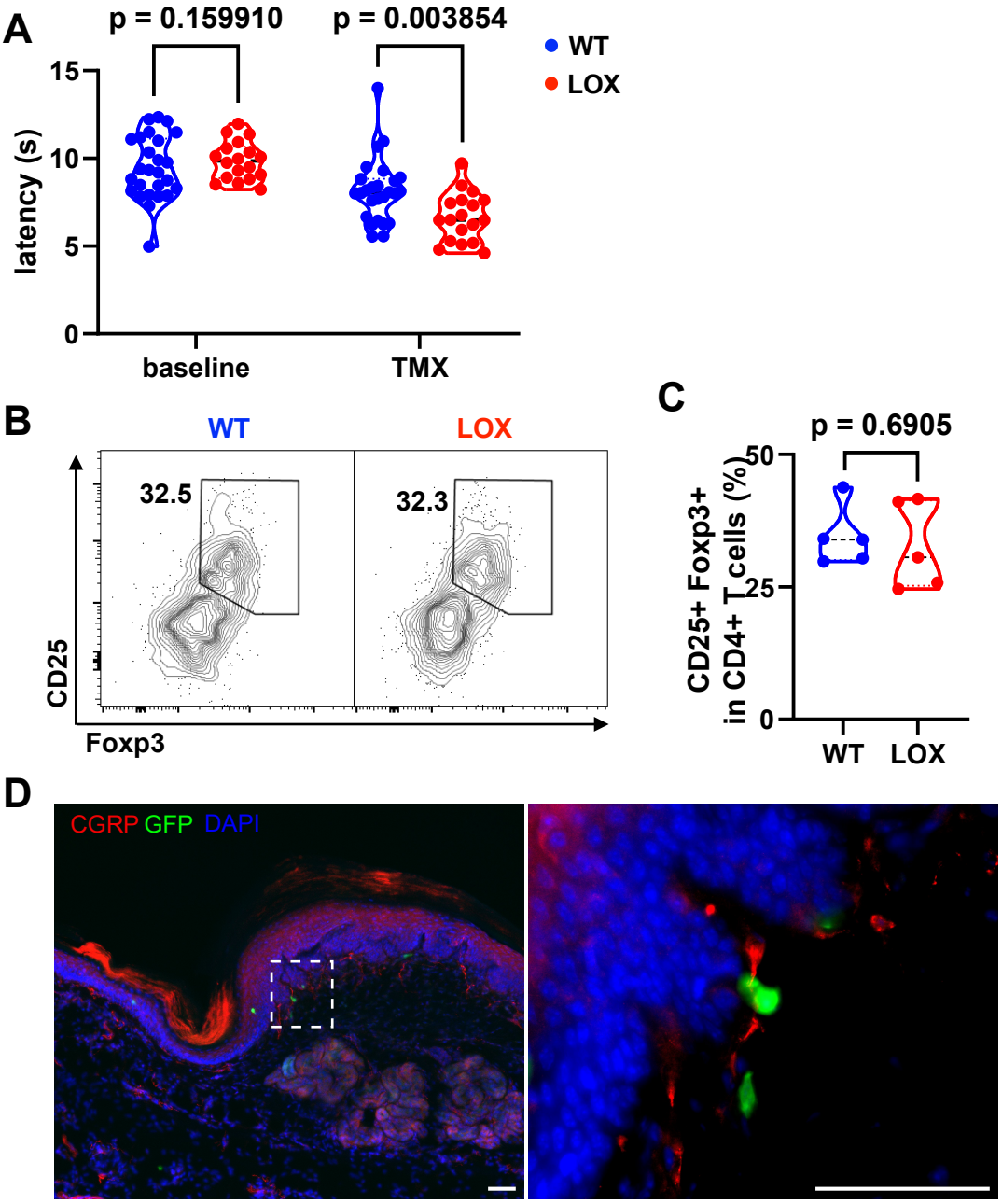
A
p = 0.159910
p = 0.003854
WT
LOX
latency (s)
15
10
5
0
baseline
TMX
B
WT
LOX
32.5
32.3
CD25
Foxp3
C
p = 0.6905
CD25+ Foxp3+
in CD4+ T cells (%)
50
25
0
WT
LOX
D
CGRP GFP DAPI

Figure 5